



## Defect studies of hydrogen-loaded thin Nb films

J. Čížek<sup>a,\*</sup>, I. Procházka<sup>a</sup>, G. Brauer<sup>b</sup>, W. Anwand<sup>b</sup>, A. Mücklich<sup>b</sup>,  
R. Kirchheim<sup>c</sup>, A. Pundt<sup>c</sup>, C. Bähz<sup>d</sup>, M. Knapp<sup>d</sup>

<sup>a</sup> Faculty of Mathematics and Physics, Charles University, Department of Low-Temperature Physics,  
V Holesovickach 2, CZ-180 00, Prague 8, Czech Republic

<sup>b</sup> Institut für Ionenstrahlphysik und Materialforschung, Forschungszentrum Rossendorf, Dresden, Germany

<sup>c</sup> Institut für Materialphysik, Universität Göttingen, Germany

<sup>d</sup> Institut of Materials Science, Darmstadt University of Technology, Germany

Available online 29 September 2005

### Abstract

Hydrogen interaction with defects in thin niobium (Nb) films was investigated using slow positron implantation spectroscopy (SPIS) combined with X-ray diffraction (XRD) and transmission electron microscopy (TEM). Thin Nb films on Si substrates were prepared using cathode beam sputtering at room temperature. Initially, the microstructure of the virgin (hydrogen-free) films was characterized. Subsequently, the films were step-by-step electrochemically charged with hydrogen and the evolution of the microstructure with increasing hydrogen concentration was monitored. Hydrogen loading leads to a significant lattice expansion which was measured by XRD. Contrary to free-standing bulk metals, thin films are highly anisotropic. The in-plane expansion is prevented because the films are clamped on the elastically hard substrate. On the other hand, the out-of-plane expansion is substantially higher than in the bulk samples. Moreover, an enhanced hydrogen solubility in the  $\alpha$ -phase was found in nanocrystalline Nb films. It was found that most of positrons in the films are trapped at open-volume defects at grain boundaries (GBs). These defects represent trapping sites also for hydrogen atoms. Hydrogen trapping at vacancy-like defects like GBs leads to a local increase of the electron density and is reflected by a pronounced decrease of the  $S$  parameter in the hydrogen-loaded samples. In addition, it was found that new defects are introduced at higher concentrations of hydrogen due to the formation of NbH ( $\beta$ -phase) particles.

© 2005 Elsevier B.V. All rights reserved.

**Keywords:** Niobium films; Hydrogen; Slow positron implantation spectroscopy; Doppler broadening; X-ray diffraction

### 1. Introduction

The behavior of hydrogen in a host metal lattice can be significantly influenced by hydrogen interaction with lattice defects. For example, it is well known that hydrogen can be trapped at vacancies [1] and

\* Corresponding author. Tel.: +420 2 2191 2788;  
fax: +420 2 2191 2567.  
E-mail address: [jcizek@mbox.troja.mff.cuni.cz](mailto:jcizek@mbox.troja.mff.cuni.cz) (J. Čížek).

dislocations [2]. Moreover, hydrogen is not only trapped at existing defects but new defects can also be generated by hydrogen loading. Recently it has been found that vacancies surrounded by four hydrogen atoms were created in bulk Nb by electrochemical hydrogen charging [3]. A strong interaction of hydrogen with defects makes defect studies of hydrogen-loaded samples highly important for an understanding of the hydrogen behavior in metals. Positron annihilation spectroscopy (PAS) is a well-developed non-destructive technique with a high sensitivity to open-volume defects [4]. Thus, PAS represents an ideal tool for the investigation of hydrogen-defect interactions as well as the characterization of hydrogen-induced defects. Indeed, PAS was employed successfully in investigations of hydrogen-induced defects in bulk Nb [3]. Hydrogen absorption leads to a significant increase of the volume and thereby also to a lattice expansion of the sample. The expansion is isotropic in case of free-standing bulk metals. Contrary to a bulk material, a thin film is clamped usually on an elastically hard substrate. It prevents the in-plane expansion, while the out-of-plane expansion is remarkably larger compared to a free-standing bulk metal. As a consequence hydrogen-induced effects in thin films may differ substantially from those in corresponding bulk materials. Because of this important difference it is highly desirable to equate the hydrogen behavior in thin films with that in bulk samples.

The aim of the present work was the investigation of microstructure changes in hydrogen-loaded thin Nb film. We chose Nb because the phase diagram of Nb–H system is relatively simple and well-documented [5]. It is thus advantageous for investigations of the influence of defects on the hydrogen behavior. At room temperature the Nb–H system represents a single phase solid solution (so called  $\alpha$ -phase) up to a hydrogen concentration  $x_H = 0.06$  [atom ratio H/Nb]. At higher hydrogen concentrations the system becomes a mechanical mixture of two phases: the  $\alpha$ -phase and the hydrogen-rich  $\beta$ -phase which is an orthorhombic distortion of the Nb lattice. In the  $\alpha$ -phase, hydrogen occupies the tetrahedral interstitial positions in the bcc Nb lattice. In the present work, the thin Nb films were step-by-step electrochemically loaded with hydrogen in the range from  $x_H = 0$  to 1.0 and the development of the microstructure was

investigated. Defect studies of thin films were performed by slow positron implantation spectroscopy (SPIS) with measurement of Doppler broadening (DB) of the annihilation line. Hydrogen-induced lattice expansion was detected by X-ray diffraction (XRD). These techniques were combined with a direct observation of the microstructure by transmission electron microscopy (TEM).

## 2. Experimental details

Thin Nb films were prepared in an UHV chamber using cathode beam sputtering at room temperature on polished (1 0 0)Si substrates. The thickness of the films was determined by profilometry and by TEM as 1100(50) and 1120(20) nm, respectively. The surface of all samples was covered with a 20 nm thick Pd cap in order to prevent oxidation and to facilitate hydrogen absorption. The samples were step-by-step loaded with hydrogen by electrochemical charging, see ref. [2] for details. The charging was done in a galvanic cell by constant current pulses (charge density amounts  $3 \times 10^{-3} \text{ mA mm}^{-2}$ ) using a Pt counter electrode, while the loaded sample is used as a working electrode. We used a mixture of  $\text{H}_3\text{PO}_4$  (85%) and glycerin (85%) in the ratio 1:1 as electrolyte. In order to prevent hydrogen losses, oxygen was removed from the electrolyte by slow rate bubbling with Ar for 24 h prior to the electrochemical charging. The hydrogen concentration in the sample was calculated from Faraday's law [2]. The voltage between the charged sample and a reference Ag/AgCl electrode was measured. This voltage (so called electromotive force, EMF) is related to the chemical potential of hydrogen (see ref. [2] for details) and may be used for an independent determination of phase boundaries in the studied films. The EMF measurements were carried out with an impedance converter of high input resistance and a digital voltmeter connected to a computer. The SPIS studies of defects in thin films were performed at the magnetically guided positron beam "SPONSOR" [6] with positron energy adjustable from 0.03 to 36 keV. Energy spectra of annihilation gamma rays were measured by a Ge detector with an energy resolution of  $1.09 \pm 0.01 \text{ keV}$  at 511 keV. Doppler broadening of the annihilation peak was analyzed using the  $S$  parameter [4] (i.e. the

central area of the peak divided by the net peak area) which is a measure of the fraction of positrons annihilating with low momentum electrons. The central area borders were selected so that they cover momentum range from 0 to  $7 \times 10^{-3} m_0c$ . Texture measurements were performed on a four-axis Philips X'pert MPD diffractometer using Co K $\alpha$  radiation. XRD measurements of the hydrogen-induced lattice expansion were performed at Hasylab (DESY) using synchrotron radiation with wavelength  $\lambda = 1.12 \text{ \AA}$ . The lattice expansion was measured in the out-of-plane direction (i.e. in the direction perpendicular to the film surface, which corresponds to  $\psi = 0^\circ$ ) and in the direction tilted by  $\psi = 60^\circ$  with respect to the normal to the surface. In such a way, we obtained information about the anisotropy of the film expansion. Diffraction profiles were fitted by the Pearson VII function. TEM studies were performed with a Philips CM300SuperTWIN microscope operating at 300 kV. Thin foils for cross-sectional TEM were produced by conventional preparation using Gatan precision ion polishing system (PIPS).

### 3. Results and discussion

A bright-field TEM image (cross-section) of the virgin film (i.e. without hydrogen) is shown in Fig. 1a. The sample exhibits “column-like” elongated grains. The widths of the columns do not exceed 100 nm.

Typically they lie around 50 nm. A high resolution image of a column is shown in Fig. 1b. The columns are divided horizontally into two “generations” of sub-columns with a height being approximately the half of the film thickness. The “first generation” sub-columns are situated close to the Si substrate, while the “second generation” sub-columns are situated close to the film surface.

Texture measurements showed that the film exhibits a strong 1 1 0 texture, i.e. grains are oriented predominantly with  $\{1 1 0\}$  planes parallel to the surface. However, the lateral orientation of grains is random. The diffraction profile shape of (1 1 0)Nb reflection measured on the virgin film is plotted in Fig. 2a and b for the out-of-plane direction ( $\psi = 0^\circ$ ) and the direction tilted  $\psi = 60^\circ$  with respect to the normal to the surface. The profiles shown in Fig. 2a and b are a superposition of Nb(1 1 0) reflection from the Nb layer and a weak Pd(1 1 1) reflection coming from the Pd cap. Moreover, one can see from Fig. 2a that the reflection for  $\psi = 0^\circ$  is asymmetric and it must be fitted by three different contributions: a weak and broad reflection from the Pd cap and two different contributions from the Nb layer corresponding to the inter-planar distance 2.391(2) and 2.362(2) Å. Taking into account the results of TEM observations discussed above, it indicates that the distance  $d_{1 1 0}$  between the  $\{1 1 0\}$  planes in the “first generation” sub-columns (close to the Si substrate) and in the “second generation” sub-columns (close to the film

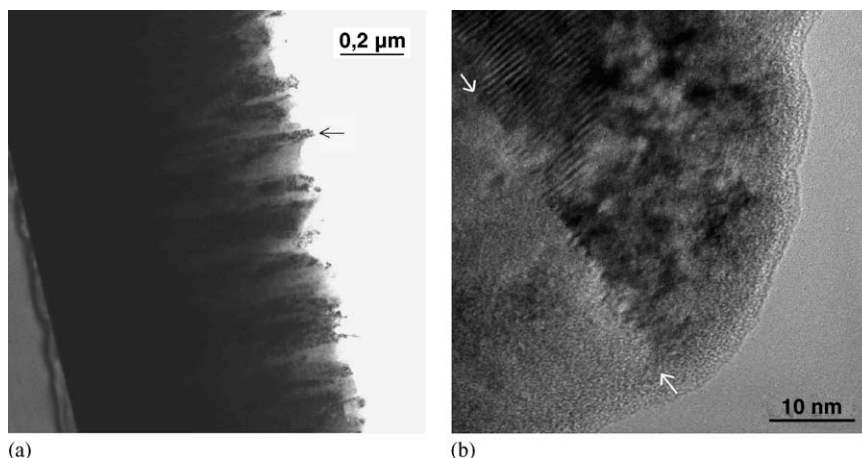


Fig. 1. (a) Bright-field TEM image of the virgin film and (b) high resolution image of the region indicated in the left panel by an arrow. The interface between grains is indicated by white arrows.

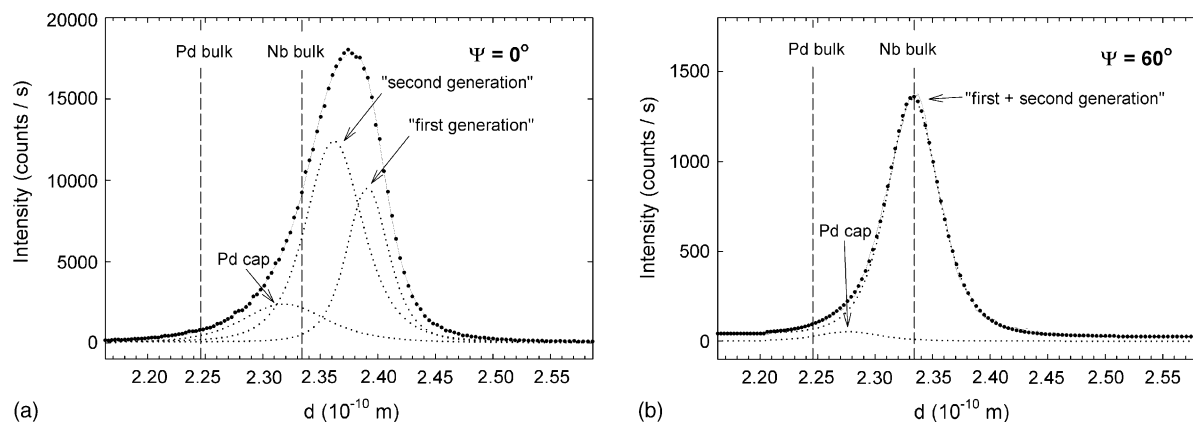


Fig. 2. XRD diffraction profile for the virgin film (a) in direction out-of-plane,  $\Psi = 0^\circ$  and (b) in direction tilted  $\Psi = 60^\circ$  with respect to the normal to the surface. Fit of the experimental points is plotted by the solid lines, while the dotted lines show the individual reflections which contribute to the profile. The distance between the  $\{110\}$  and  $\{111\}$  planes in bulk Nb and Pd, respectively, is indicated by the dashed vertical lines.

surface) differs. It should be mentioned that the distance between the  $\{110\}$  planes in bulk Nb is  $d_{110} = 2.3338 \text{ \AA}$  [7] (the dashed line in Fig. 2a and b). Similarly the distance between the  $\{111\}$  planes in bulk Pd is indicated in Fig. 2a and b by another dashed line. It is clear that the out-of-plane distance  $d_{110}$  in the Nb layer (both kinds of sub-columns) as well as  $d_{111}$  in the Pd over-layer are significantly higher than in the corresponding bulk materials. Moreover, we have found that  $d_{110}$  decreases with increasing tilting angle  $\Psi$ , see the text below. Such experimental findings can be explained by compressive stresses in the in-plane direction caused by mismatch in atomic spacing between the Nb film and the Si substrate. It leads to anisotropy of  $d_{110}$ , so that  $d_{110}$  is higher than that for bulk Nb in the out-of-plane direction, while in the in-plane direction it is smaller. The “first generation” sub-columns are attached directly to the Si substrate which leads to the highest mismatch of the lattice constants. On the other hand, the “second generation” sub-columns grow on the “first generation” and the mismatch is, therefore, smaller. Thus, we can attribute  $d_{110} = 2.391(2) \text{ \AA}$  to the “first generation” sub-columns where the compressive stresses are higher, while  $d_{110} = 2.362(2) \text{ \AA}$  (closer to the Nb bulk value) can be attributed to the “second generation” sub-columns which are more relaxed. The distance between the  $\{110\}$  planes in the direction tilted  $\Psi = 60^\circ$  with respect to normal to the surface is remarkably smaller compared to the out-of-plane direction and practically coincides with  $d_{110}$  for bulk

Nb, see Fig. 2b. The  $d_{110}$  distances for the two generations of sub-columns lie in this case too close to each other in order to separate their contributions in XRD spectrum. The inter-planar distances  $d_{110}$  in the out-of-plane direction for both kinds of sub-columns and  $d_{110}$  for the direction  $\Psi = 60^\circ$  are plotted in Fig. 3a as a function of  $x_H$ . One can see in the figure that  $d_{110}$  exhibits an increase with  $x_H$  which is approximately linear in the  $\alpha$ -phase field. However, there is a change of slope of the film expansion in the out-of-plane direction at  $x_H = 0.06$ , see Fig. 3a. Formation of the  $\beta$ -phase starts above  $x_H = 0.25$ . It is demonstrated clearly in the direction  $\Psi = 60^\circ$  by the appearance of a new diffraction profile which corresponds to the  $(200)$  reflection from the  $\beta$ -phase. Thus, in the case of  $\beta$ -phase the inter-planar distance shown in Fig. 3a corresponds to the distance between the  $\{200\}$  planes. In the out-of-plane direction it was not possible to separate the contribution which comes from the  $\beta$ -phase because of a more complicated structure of the diffraction profile. Nevertheless, the start of the  $\beta$ -phase formation is indicated by an increase of the width of this reflection. In the range from  $x_H = 0.25$  to  $0.60$  the film represents a mechanical mixture of the  $\alpha$ -phase and the hydrogen-rich  $\beta$ -phase. The volume fraction of the  $\beta$ -phase increases with  $x_H$ . Eventually, at higher concentrations  $x_H > 0.60$ , the film is completely transformed into the  $\beta$ -phase. The maximum hydrogen solubility in bulk Nb at room temperature is  $0.06$ . Hence the film exhibits four times higher apparent solubility of

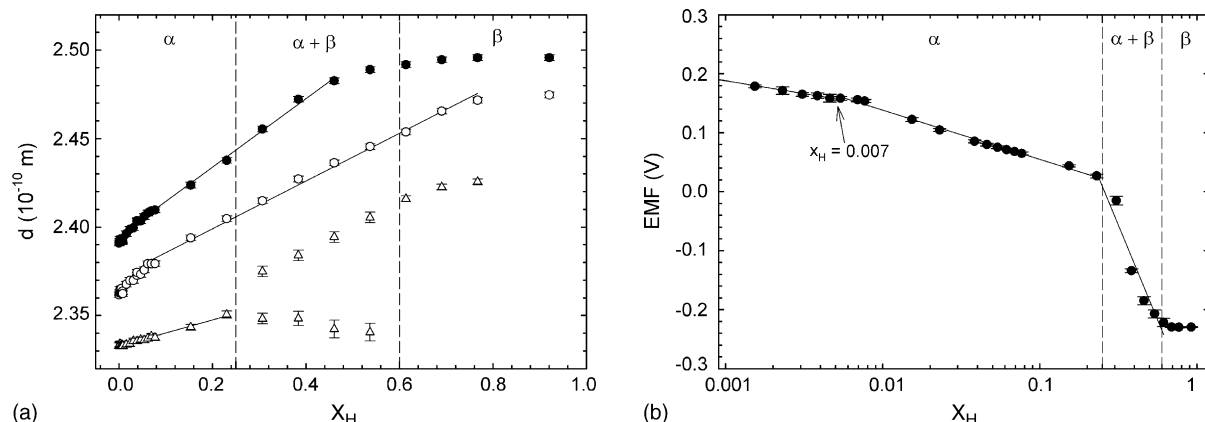


Fig. 3. (a) Dependence of the inter-planar distance  $d$  on hydrogen concentration  $x_H$  in the film. Full circles,  $d_{110}$  “first generation” sub-columns,  $\Psi = 0^\circ$ ; open circles,  $d_{110}$  “second generation” sub-columns,  $\Psi = 0^\circ$ ; gray triangles,  $d_{110}$ ,  $\Psi = 60^\circ$ ; open triangles,  $d_{200}$ ,  $\beta$ -phase,  $\Psi = 60^\circ$  and (b) dependence of EMF on hydrogen concentration. Positions of phase boundaries are indicated by vertical dashed lines.

hydrogen in the  $\alpha$ -phase compared to bulk Nb. The extended apparent hydrogen solubility could be due to nanocrystalline grains. It leads to a significant volume fraction of grain boundaries (GBs) which can accumulate more hydrogen atoms. Note that enhanced apparent hydrogen solubility in thin Nb films has been already reported in ref. [8].

The dependence of the EMF on  $x_H$  is plotted in Fig. 3b. One can see that EMF exhibits a dramatic decrease in the interval from  $x_H = 0.25$  to 0.60 which

appears in correlation with the formation of the  $\beta$ -phase. It is in a good agreement with the positions of the phase boundaries determined by XRD. In addition there is a change of slope of the EMF dependence at  $x_H = 0.007$ . This effect will be discussed later in connection with SPIS results. The relative lattice expansion  $\Delta(x_H) = [d(x_H) - d_0]/d_0$ , where  $d_0$  and  $d(x_H)$  represent inter-planar distance in the virgin sample and in the sample loaded to hydrogen concentration  $x_H$ , respectively, is plotted in Fig. 4 as

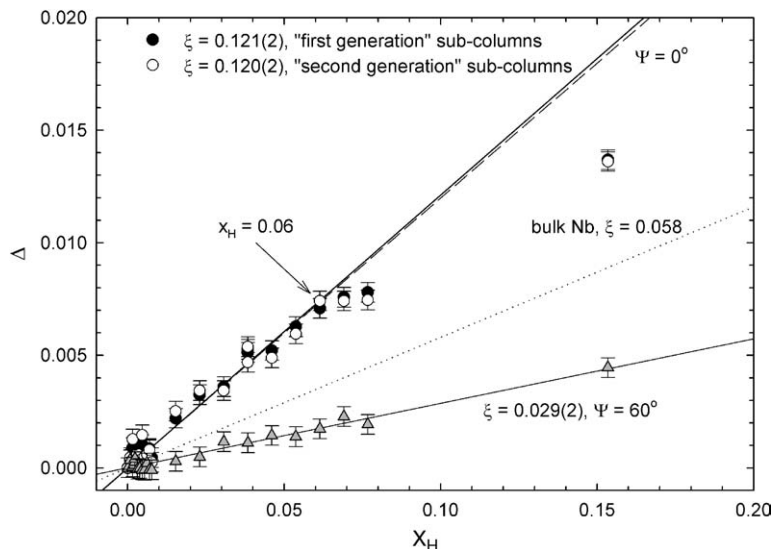


Fig. 4. Hydrogen-induced relative lattice expansion  $\Delta$  as a function of hydrogen concentration  $x_H$ . Dependence of the inter-planar distance  $d$  on hydrogen concentration  $x_H$  in the film. Full circles, “first generation” sub-columns,  $\Psi = 0^\circ$ ; open circles, “second generation” sub-columns,  $\Psi = 0^\circ$ ; gray triangles,  $\Psi = 60^\circ$ . The relative lattice expansion for bulk Nb is shown by dotted line.

a function of  $x_H$  in the  $\alpha$ -phase field (i.e. for  $x_H < 0.25$ ). The relative lattice expansion in bulk Nb is isotropic and in the  $\alpha$ -phase region it is directly proportional to hydrogen concentration, i.e.  $\Delta(x_H) = \xi x_H$ . The material constant  $\xi = 0.058$  can be found in literature for bulk Nb [9]. On the other hand, the in-plane expansion of thin film is prevented by clamping on the elastically hard substrate suggesting that film expansion in the in-plane direction is very small (if any). XRD studies of the hydrogen-loaded thin films turned out that the out-of-plane expansion is substantially larger than in a free-standing bulk sample [10]. It can be seen from Fig. 4 that  $\Delta(x_H)$  in the out-of-plane direction is the same for both generations of sub-columns and it is significantly higher than in bulk Nb (shown by dotted line). On the other hand,  $\Delta(x_H)$  in the direction  $\Psi = 60^\circ$  is smaller than in bulk Nb. Moreover, there is a change of slope of the out-of-plane expansion at  $x_H = 0.06$ . Such an effect does not occur in the bulk Nb and indicates some change of mechanism of the film expansion.

The dependence of the  $S$  parameter on positron energy  $E$  for the virgin film and for selected hydrogen concentrations are plotted in Fig. 5a. A drop of  $S$  at low energies is due to positron annihilations inside the Pd cap. It was confirmed by the measurement of a reference 1000 nm thick Pd film sputtered under the same conditions as the Nb films. Increasing fraction of positrons annihilating inside the Nb layer is reflected by an increase of  $S$  starting from  $E = 1$  keV. In the

interval from 4 to 22 keV virtually all positrons annihilate inside the Nb layer and  $S$  remains approximately constant. Eventually at high energies  $E > 22$  keV some positrons penetrate into the Si substrate which leads to a further increase of  $S$ . The solid lines in Fig. 5a represent a fit performed using VEPFIT software package [11] assuming three layers (i.e. Pd cap, Nb layer and Si substrate). SPIS measurement of a reference well-annealed (defect-free) bulk Nb revealed the bulk value of the  $S$  parameter 0.5095(3) and the positron diffusion length of 310(10) nm. From Fig. 5a it is clear that the  $S$  parameter for the Nb layer,  $S_{Nb}$ , in the virgin sample is substantially higher than the bulk value for defect-free Nb. The effective positron diffusion length for the Nb layer obtained from fit of the  $S(E)$  curve for the virgin film is only 20 nm. Thus, we can conclude that the virgin film exhibits a high density of defects. From comparison with TEM results we can see that the width of the columns determined by TEM is about three times smaller than the diffusion length of positrons in defect-free Nb, while it is of the order of magnitude as the effective positron diffusion length for the Nb layer. Thus, there is a high probability for any free positron to diffuse to a grain boundary, i.e. to the interface between the columns, and to be trapped at an open-volume defect there. Therefore, we assume that most positrons in the virgin film are trapped at the open-volume defects at the interfaces between the columns.

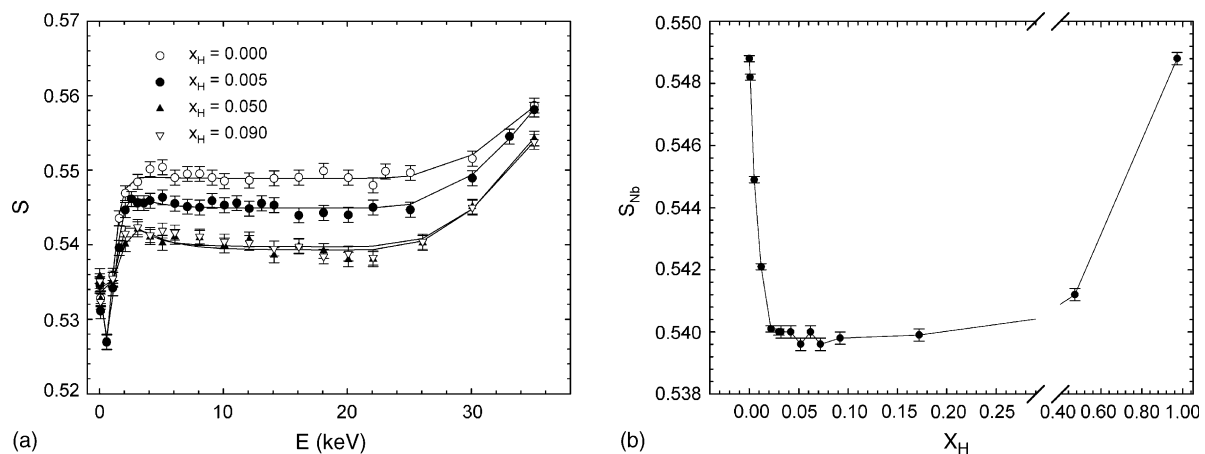


Fig. 5. (a) Selected  $S(E)$  curves for the virgin film and the film loaded to various concentrations of hydrogen and (b) dependence of the  $S$  parameter for Nb layer,  $S_{Nb}$ , obtained from fit of the  $S(E)$  curves on hydrogen concentration.

One can see in Fig. 5a that  $S_{\text{Nb}}$  decreases for hydrogen-loaded films. It indicates that similarly to positrons also hydrogen is trapped at the open-volume defects at GBs. It was proved both by theoretical calculations and experimentally that a vacancy-like defect with one or more hydrogen atoms is still able to trap positrons [3]. However, the presence of hydrogen bound to such defect leads to an increase of the local electron density at the defect and, thereby, to a decrease of the lifetime of trapped positrons. In addition, the positron binding energy to the defect becomes lower. As a consequence, the overlap of positron wave function with high momentum core electrons increases and leads to a decrease of the  $S$  parameter. The dependence of  $S_{\text{Nb}}$  obtained from fit of the  $S(E)$  curves on  $x_{\text{H}}$  is plotted in Fig. 5b. Going from the virgin film,  $S_{\text{Nb}}$  decreases rapidly indicating that hydrogen firstly fills gradually the open-volume defects at GBs. Above  $x_{\text{H}} = 0.02$ ,  $S_{\text{Nb}}$  reaches a plateau value suggesting that all the available open-volume traps at GBs are already filled and the local concentration of hydrogen in vicinity of the defects reaches a steady state value. A high mobility of hydrogen in Nb at room temperature [3] ensures that if there is any open-volume trap available, then the hydrogen atom likely finds it. Hence, at low concentrations of hydrogen practically all hydrogen atoms may be trapped at the defects at GBs. It is clear that the chemical potential of hydrogen situated at GB differs from that of hydrogen in the regular tetrahedral interstitial position inside grain. It should be reflected by a change of slope of the EMF dependence when hydrogen starts to occupy the interstitial positions inside grain. In view of these facts, we can, therefore, assign the change of slope of the EMF dependence observed at  $x_{\text{H}} = 0.007$  (Fig. 3b) to hydrogen concentration from which hydrogen is not situated exclusively at GBs but starts to occupy also the regular tetrahedral interstitial positions inside the grains. The formation of the  $\beta$ -phase takes place at  $x_{\text{H}} > 0.25$ . It is known that dislocation loops may be emitted by growing particles of hydrides [12]. In addition, positrons can be trapped at misfit defects at the interface between a  $\beta$ -phase precipitate and the matrix. Indeed, as one can see in Fig. 5b,  $S_{\text{Nb}}$  exhibits an increase at  $x_{\text{H}} > 0.25$  due to formation the  $\beta$ -phase particles.

Thus, we can conclude that the formation of  $\beta$ -phase particles leads to an introduction of new open-volume defects.

#### 4. Conclusions

In the present work we performed defect studies of hydrogen-loaded nanocrystalline thin Nb film of a thickness  $\approx 1.1 \mu\text{m}$ . The film exhibits a high density of defects already in the virgin state. Most of positrons annihilate from the trapped state at open-volume defects at grain boundaries. It was found that apparent hydrogen solubility in the  $\alpha$ -phase in the film is four times higher compared to bulk Nb. Hydrogen-induced lattice expansion of the film exhibits a strong anisotropy: the out-of-plane expansion is significantly higher than in bulk Nb, while the expansion in direction tilted by  $\Psi = 60^\circ$  with respect to normal to the film surface is remarkably smaller. SPIS measurements revealed that hydrogen is trapped at open-volume defects at grain boundaries which is seen by a decrease of the  $S$  parameter. No formation of new defects was found in the  $\alpha$ -phase region. On the other hand, formation of  $\beta$ -phase particles leads to an increase of defect density.

#### Acknowledgements

Financial support from The Czech Science Foundation (project no. 202/05/0074), The Ministry of Education of The Czech Republic (project nos. 1K03025 and MS 0021620834), The HASYLAB and The Alexander von Humboldt Foundation is highly acknowledged.

#### References

- [1] B. Lengeler, S. Mantl, W. Triftshäuser, J. Phys. F 8 (1978) 1691.
- [2] R. Kircheim, Prog. Mater. Sci. 32 (1988) 261.
- [3] J. Čížek, I. Procházka, F. Bečvář, R. Kužel, M. Cieslar, G. Brauer, W. Anwand, R. Kirchheim, A. Pundt, Phys. Rev. B 69 (2004) 224106.
- [4] P. Hautojärvi, C.J. Corbel, in: A. Dupasquier, A.P. Mills, Jr. (Eds.), Positron Spectroscopy of Solids, IOS, Amsterdam, 1995, p. 491.

- [5] T. Schober, H. Wenzl, in: G. Alefeld, J. Völkl (Eds.), *Hydrogen in Metals II*, Topics in Applied Physics, vol. 29, Springer, Berlin, 1978, p. 32.
- [6] W. Anwand, H.-R. Kissener, G. Brauer, *Acta Phys. Pol. A* 88 (1995) 7.
- [7] ICDD (International Centrum for Diffraction Data) powder diffraction pattern database PDF-2.
- [8] S. Mochlecke, C.F. Majkrzak, M. Strongin, *Phys. Rev. B* 31 (1985) 6804.
- [9] H. Peisl, in: G. Alefeld, J. Völkl (Eds.), *Hydrogen in Metals I*, Topics in Applied Physics, vol. 28, Springer, Berlin, 1978, p. 53.
- [10] U. Laudahn, A. Pundt, M. Bicker, U.V. Hülsen, U. Geyer, T. Wagner, R. Kirchheim, *J. Alloys Compd.* 293–295 (1999) 490.
- [11] A. van Veen, H. Schut, M. Clement, J. de Nijs, A. Kruseman, M. Ijpma, *Appl. Surf. Sci.* 85 (1995) 216.
- [12] C. Borchers, U. Laudahn, A. Pundt, S. Fähler, H.U. Krebs, R. Kirchheim, *Philos. Mag. A* 80 (2000) 543.